Tests of the demodulating CCDs for the SPHERE / ZIMPOL imaging polarimeter

Hans-Martin Schmid[a], Mark Downing[b], Ronald Roelfsema[c], Andreas Bazzon[a], Daniel Gisler[a], Johan Pragt[c], Claudio Cumani[b], Bernardo Salasnich[d], Alexey Pavlov[e], Andrea Baruffolo[d], Jean-Luc Beuzit[f], Anne Costille[f], Sebastian Deiries[b], Kjetil Dohlen[g], Carsten Dominik[h], Eddy Elswijk[c], Markus Feldt[e], Markus Kasper[b], David Mouillet[f], Christian Thalmann[h], Francois Wildi[i]

[a]ETH Zurich, Institute of Astronomy, Wolfgang-Pauli-Str. 27, 8093 Zurich, Switzerland;
[b]ESO, Karl-Schwarzschild-Str. 2, 85748 Garching, Germany;
[c]NOVA Optical-Infrared Group at ASTRON, 7991 PD Dwingeloo, The Netherlands;
[d]INAF, Osservatorio Astronomico di Padova, Vicolo dell'Osservatorio 5, 35122 Padova, Italy;
[e]Max-Planck-Institut für Astronomie, Königstuhl 17, 69117 Heidelberg, Germany;
[f]UJF-Grenoble, Inst. de Planétologie et d'Astrophys. de Grenoble (IPAG), 38041 Grenoble, France;
[g]LAM, Observatoire de Marseille, 38 rue Frédéric Joliot-Curie, 13388 Marseille, France;
[h]Astronomical Institute "Anton Pannekoek", 1098 SJ Amsterdam, The Netherlands;
[i]Observatoire Astronomique de l'Universite de Geneve, 1290 Sauverny, Switzerland

ABSTRACT

The imaging polarimeter ZIMPOL is one of three focal plane instruments of the SPHERE / VLT planet finder. ZIMPOL measures the linear polarization based on a fast modulation – demodulation principle using a charge-shifting technique on a masked CCD for separating the photons with opposite polarization direction. This paper describes the on-chip demodulation and the different detector read-out modes which are implemented for the ZIMPOL polarimeter. Test results are presented which allow an evaluation of the performance of the ZIMPOL CCD detectors. The achievable polarization efficiency is close to expectation and the charge trap correction with the two-phase demodulation mode works well. Other detector effects like bias level variations and read-out patterns can be corrected in the data reduction process. The tests demonstrate that the demodulating CCDs fulfill the requirements for the SPHERE project.

1. INTRODUCTION: THE SPHERE PROJECT

The SPHERE "Planet Finder" instrument is a 2nd generation VLT instrument which should become in 2013 one of the most sensitive ground based instruments for the search and investigation of extra-solar planets. The challenge of this instrument is the detection of a planet very close (of the order 0.1 arcsec) to a bright star despite an extremely large contrast between planet and star. Expected contrast ratios are 10^{-4} to 10^{-6} in the near-IR for the detection of the emission of young, bright giant planets and 10^{-8} in the visual for the detection of reflected light from old, cool planets. To fulfill these science goals, the instrument will include the following main features: an extreme adaptive optics (AO) system, stellar coronagraphs, and three differential imagers[1,2]. Figure 1 shows a block diagram of the SPHERE instrument.

The heart of the instrument is the adaptive optics (AO) system, which will correct for the variable wave-front distortions introduced by Earth's atmosphere and the static aberrations of the instrument. For this a visual Shack-Hartmann wave-front sensor (WFS) measures the wave distortions of a bright (R < 9.5 mag) star. This drives then a control loop for a tip-tilt and a deformable mirror with 41×41 actuators with a control frequency of about 1.3 kHz. The AO system will provide a very good correction with a Strehl ratio of about 0.5 at $\lambda = 0.8$ μm and about 0.85 at 1.6 μm. The spatial resolution provided by VLT / SPHERE is 20 mas (milli-arcsec) for a wavelength of $\lambda = 0.8$ μm and 40 mas for 1.6 μm.

In a second step a visual or near-IR stellar coronagraph attenuates the light from the bright central star in order to allow for higher contrast performance and to avoid heavy saturation of the detector. Several types of exchangeable coronagraphs are implemented: classical Lyot coronagraphs, four quadrant phase masks, and for the near-IR also apodized Lyot coronagraphs.

Despite AO system and stellar coronagraph the faint signal of the planet will be orders of magnitudes fainter than the residual, variable speckle halo from the central star. Therefore differential imaging is required as a third step to enhance further the contrast. SPHERE will use differential spectral imaging and polarimetric differential imaging techniques and both can be combined with angular differential imaging. Spectral differential imaging searches for spectral features which are present in the planet spectrum but not in the star spectrum. Well suited for this purpose are the strong methane bands in the 0.95 μm to 1.7 μm wavelength region. The two near-IR focal plane instruments of SPHERE use this method: the infrared dual beam spectrograph IRDIS can take simultaneous images inside and outside strong CH_4 bands and the integral field spectrograph (IFS) will take low resolution spectra for each point in the field of view. IRDIS includes also complementary spectroscopic and polarimetric modes for the near-IR.

ZIMPOL, the Zurich imaging polarimeter is optimized for differential polarimetry in the visible. Polarimetry is useful for observations of extra-solar planets and circumstellar disks because the light reflected from planets and disks is polarized while no polarization is expected from the central star[3]. The polarization is expected to be particularly high at short wavelengths < 1 μm due to Rayleigh scattering by atoms and molecules and scattering by aerosol particles in planetary atmospheres and by dust grains in circumstellar disks. Therefore ZIMPOL is operating at short wavelengths between 0.50 and 0.90 μm. ZIMPOL is a very innovative concept for imaging polarimetry using fast modulation / demodulation based on CCD detector technology. ZIMPOL provides also (non-polarimetric) high contrast imaging in broad and narrow band filters.

In this paper we describe the properties of the CCDs used in ZIMPOL / SPHERE and their operation and performance for polarimetric measurements. In Section 2 we introduced the basic ZIMPOL principles of the on-chip demodulation, followed by a description of the CCD operation modes in Section 3. Then we discuss the polarimetric efficiency of the system in Section 4 and the CCD charge trap problem in Section 5. Bias, dark current, read-out patterns and charge smearing effects are treated in Sections 6 and 7. In Section 8 we present our conclusions
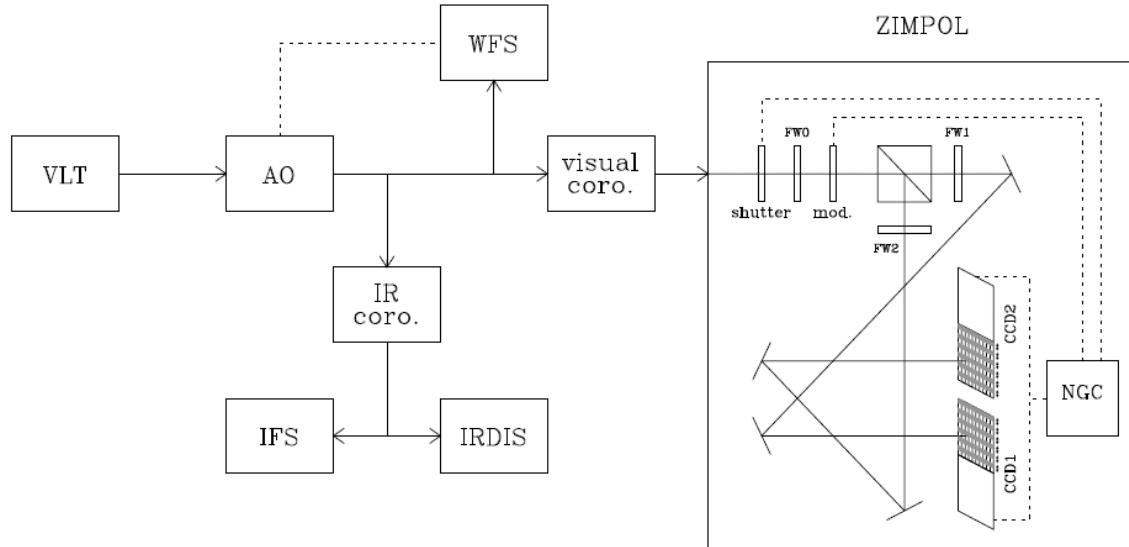
**Figure 1.** Block diagram giving an outline of the different subsystems of the SPHERE instrument (VLT: very large telescope, AO: adaptive optics system, WFS: wave front sensor, IR/visual coro: coronagraphs, IFS: integral field spectrograph, IRDIS: infrared dual beam spectrograph, and ZIMPOL: Zurich imaging polarimeter). The components controlled by the NGC, ESO's new general detector controller, are highlighted in the ZIMPOL box.

2. ZIMPOL: A DEMODULATING CCD-DETECTOR FOR IMAGING POLARIMETRY

2.1 ZIMPOL basic principle and development history

Atmospheric seeing variations are a main problem for high precision differential measurements from the ground. For differential polarimetry this problem can be solved with a fast polarization modulator with a modulation frequency in the kHz range, combined with an imaging photometer which demodulates the intensity signal in synchronism with the modulation. The polarization modulator and associated polarizer (polarization beam splitter) convert the degree-of-polarization signal into a fractional modulation of the intensity signal, which is then measured in a demodulating detector system by a differential intensity measurement between the two modulator states. This technique was introduced by J. Kemp[4,5] for aperture polarimetry using photoelastic modulators and single channel lock-in detector. In ZIMPOL this principle was further developed by using CCD array detectors for the demodulation by H.P. Povel[6,7]. For this "every second row" of the CCD is masked so that photo-charges created in the unmasked row during one half of the modulation cycle are shifted for the second half of the cycle to the next masked row, which is used as a temporary buffer storage. After about thousand or more modulation cycles enough photo-electrons have been accumulated so that the CCD can be read out with negligible read-out noise. The sum of the two images is proportional to the intensity, say e.g. $I = I_0 + I_{90}$, while the normalized difference is the polarization flux of one Stokes component, e.g. $Q = I_0 - I_{90}$.

Key advantages of this differential polarimetric technique:
- both images are created *simultaneously* (the modulation is faster than the seeing variations),
- both images are recorded with the *same pixels* reducing significantly flat-fielding issues
- the differential effect due to the storage of the two images in different buffer pixels can be compensated with *a demodulation phase-switch* between subsequent images,
- there are only very small *differential aberrations* between the two images with opposite polarization,
- in polarimetry the differential signal depends not on *chromatic effects* due to diffraction or speckle chromatism.

ZIMPOL has proved to be an extremely precise technique for polarimetric imaging. It is probably the most precise differential imaging technique with array detectors available today for astronomical observations. In solar applications ZIMPOL has routinely achieved a precision of better than 10^{-5} in (long slit) spectro-polarimetric mode[8]. For the VLT planet finder project, the solar ZIMPOL concept had to be adapted for higher transmission efficiencies, longer integration times, and broad band capabilities. This required the development of a new type of modulator, the use of higher quality half wave plates, and a CCD detector with more pixels and equipped with a cylindrical micro-lens array to reduce the photon loss on the stripe mask. ZIMPOL was included into the SPHERE planet finder instrument after the demonstration of the technical readiness[9] and detailed performance modeling for the detection of extra-solar planets[10]. The ZIMPOL subsystem has been assembled and tested in 2010 and 2011 at ASTRON[11,12,13] and in early 2012 it was integrated into the SPHERE instrument at IPAG in Grenoble[14].

2.2 Expected science signal and ZIMPOL detector requirements

The typical observations of ZIMPOL/SPHERE consists of the measurement of a tiny polarimetric signal in the AO corrected, coronagraphic point spread function (PSF) from the central bright star (the wave front source). For extra-solar planets the polarimetric signal is point-like while the signal is extended for circumstellar disks or other circumstellar structures. The photon flux in the dominating PSF depends strongly on distance from the central star. The flux is about a factor of 100 higher in the inner PSF at d = 0.1 – 0.3 arcsec, than in the outer PSF at d ≈ 1arcsec, and it decreases by another factor of 10 for a separation of 2 – 4 arcsec in the outer (uncorrected) halo.

Primary targets for the planet search are very bright nearby stars like α Cen or ε Eri. The photon flux in the inner PSF is at the level of 10^6 s^{-1} per 10 mas × 10 mas area (about the size of a spatial resolution element) for polarimetric imaging with a band width of 200 nm. On the other hand, the photon flux is only 10 s^{-1} for the same area, if the PSF of a star of magnitude 8 is searched at 1 arcsec separation for polarized light from a circumstellar disk. In the first case enough photons are collected in a few hours to aim for a polarimetric sensitivity of 10^{-5} by freezing the speckle noise with fast modulation, while in the second case the photon noise limit will only allow for a polarimetric sensitivity of 10^{-3} for and a slower modulation frequency is sufficient. Thus the detector system must be capable to handle a huge range in flux.

The detection of extra-solar planets in reflected (= polarized) light is very demanding because the polarization signal of the planet at a separation of 0.1 – 0.3 arcsec from the star is expected to be about 10^{-4} times smaller than the flux of the PSF at this location. Many frames must be collected until the planet polarization signal reaches a level which is higher than the photon noise. Therefore the CCD system must be optimized for high polarimetric sensitivity and high photon efficiency, while reducing as much as possible detector overheads and disturbing effects like dark current, and charge transfer problems. Beside this, the high polarimetric sensitivity of 10^{-5} requires also a good detector gain linearity.

Of course not only the detector, but all components of ZIMPOL / SPHERE must be optimized for high performance. But in this paper we concentrate on the detector aspects. For better photon efficiency the photon loss due to the masked CCD rows must be minimized. This is achieved with cylindrical micro-lenses which focus the light onto the open detector rows. Further there are two detector arms implemented in ZIMPOL in order to collect the photons from both beams of the polarization beam splitter cube (Figure 1). In both arms the identical polarimetric information is encoded, if the same filters are used in the filter wheels FW1 and FW2. Simultaneous color measurements are possible if different filters are used in the two arms. In order to reduce the complexity of the detector control, both detectors are operated fully synchronously. The two folding mirrors in front of the CCDs (Figure 1) can be used for beam dithering and field selection. Dithering allows to mitigate bad pixel effects, while off-axis field observations without bright central star on the detector relaxes the detector dynamic range requirements for low flux PSF regions at larger separations > 1.5 arcsec from the central star.

The ZIMPOL / SPHERE science goal requires also an elaborate observing strategy and accurate instrument calibrations. For the detector calibration continuum spectrum point and extended "flat field" sources are located in front of the ZIMPOL box. Further, the filter wheel FW0 contains polarization calibration components which provide full control of the polarization state of the incoming light. The polarimetric calibration of the ZIMPOL optics is discussed in [15].

2.3 CCD detector properties for ZIMPOL / SPHERE

The parameters of the ZIMPOL / SPHERE CCDs were defined after a thorough trade-off analysis of the science requirements and technical constraints. The requirements for charge shifting and high photon efficiency narrowed the range of useful CCDs to three-phase, back-illuminated devices. Very specific technical constraints for the CCD selection were set by the design and alignment of the micro-lens array and stripe mask on the CCD which is less critical for CCDs with large pixels. On the other side, there are the requirements for the charge shifting and fast readout for high frame rate which are less critical for small CCDs with fewer pixels.
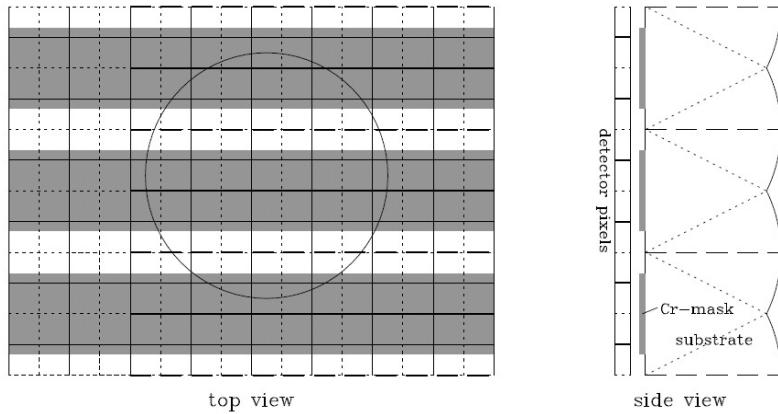
Figure 2. Schematic illustration of the CCD pixel geometry with respect to the stripe mask / micro-lens assembly seen from the top (left) and as a side cut along a pixel column and perpendicular to the cylindrical lens array (right). The physical 15×15 μm pixels are given with dotted lines and the 2×2 binned pixels by full lines on the very left. Also shown are the location of the focus line (thick dashed line) and the aperture of the cylindrical micro-lenses (full lines). The shaded areas illustrate the stripe mask. The round circle represents the PSF diameter $\lambda/D = 15$ mas (or about 120 μm on the detector) at $\lambda = 600$ nm. The substrate of the micro-lens has a thickness of 500 μm and is not drawn to scale.

Based on such considerations we selected a 4k × 2k pixel, back-illuminated, frame transfer CCDs (e2v CCD 44-82 bi) with 15 μm × 15 μm pixels. Using frame transfer CCDs reduces the detector overhead because they allow the integration during read-out of the previous frame. This detector has two read-out registers which work in parallel, each reading out half a line. The 2k × 2k image area of the CCD is large enough to operate it like a 1k × 1k pixel CCD with 2 × 2 pixel binning allowing faster read-out and providing an effective pixel size of 30 μm × 30 μm (Figure 2).

The CCDs are equipped with a stripe mask and a micro-lens array, which were developed by ETH Zurich in collaboration with the Fraunhofer IOF in Jena, Germany. The micro-lens array consists of 512 cylindrical micro-lenses etched in a 500 μm thick fused silicon substrate. Each lens has an aperture of 60 μm corresponding to four detector pixels and a length of the detector row (2048 pixels). On the backside of the substrate, there is an opaque stripe mask produced as absorbing CrOx and Cr layers. The mask consists of 512 stripes with a width of 40 μm separated by gaps of 20 μm. The position of the micro-lens focal line is about 20 μm behind the substrate centered in the gaps of the mask. The whole assembly is mounted about 10 μm above the CCD, so that the open gaps of the mask are aligned parallel to the pixel rows and the focal lines lay in the middle of the open pixel row pairs of the CCD (Figure 2). The stripe mask – micro lens device was aligned and fixed with running CCD in order to ensure an alignment precision of better than 2 μm with respect to the pixel rows.

This design of a demodulating CCD detector yields two pixel planes, the open and covered rows or after charge shifting the I_0 and I_{90} polarization direction, with 511 × 1024 pixels each (one row is lost due to the charge shifting). This means that the sampling is twice as good in the row direction when compared to the column direction. The detector sky field of view is about 3.5 × 3.5 arcsec. This provides one detector row per 7 mas for the I_0 and I_{90} frames and one detector column for every 3.5 mas for both images planes. The 7 mas sampling is sufficient for the spatial resolution of $\lambda/D = 15$ mas at 600 nm while in row direction a substantial oversampling is obtained. The optical system is designed for a round field of view with 8 arcsec diameter centered on the central star. With the tip-tilt mirrors in front of the CCDs it is possible to observe off-axis field without having the bright star on the detector. This allows for much longer integrations in off-axis fields without causing strong detector saturation.

3. CCD OPERATION MODES

3.1 Tasks of the CCD controller

The two ZIMPOL CCDs are controlled strictly in parallel with ESO's new general detector controller (NGC). The frame transfer CCDs perform at the same time the integration / demodulation in the image area while the preceding image in the shielded read-out area is read via two registers. Besides this, the CCD controller provides also time signals for the shutter and the polarization modulator (Figure 1). We highlight some special features of the ZIMPOL CCD control:

- During the integration the CCDs need to perform the polarimetric demodulation in the image area by shifting the charges up and down by two rows (one binned row) synchronously with the polarization modulation.

- Fast modulation with a cycle frequency of 967.5 Hz and slow modulation with 26.97 Hz are implemented for high and low flux applications. One cycle includes an integration phase during the first half of the cycle, a fast row shift, a second integration phase, and a fast row shift in opposite direction. Consecutive frames are recorded with alternating shift phases for the compensation of charge transfer effects (e.g. first shift sequence up – down then down – up or vice versa).

- Read-out of the previous image in the read-out area takes place during the integration / demodulation. The registered frames includes pre- and overscan pixels for a better assessment of the bias level. The read-out of a line is either stopped or completed before the row shift in the image area takes place to avoid electronic pick-up noise in the data. When the full frame is registered then the integration / demodulation in the image area continues until the end of the integration time.

- A fast frame transfer shifts the image after the integration / demodulation into the light protected read-out area. If the shutter is enabled then it interrupts the illumination during the frame transfer to avoid frame transfer smearing in the image.
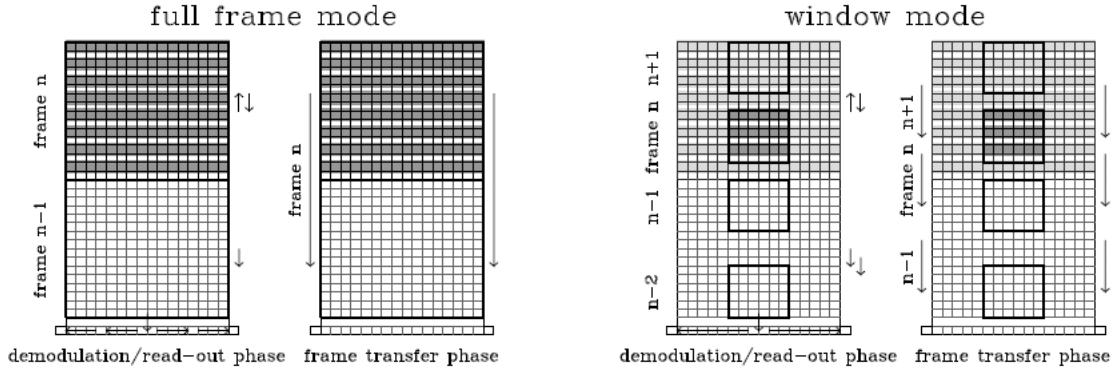
Figure 3. Schematic illustration of the detector modes for fast polarimetry for full frame read-out and window read-out. In full frame mode only half a line is read during half a cycle, thus the read out process takes place during the first 1024 full modulation cycles. In window mode one full line is read during half a cycle. The partial frame transfer shifts three window frames on the CCD.

3.2 Parameters for different detector modes

Three polarimetric detector modes are implemented for ZIMPOL to cover the needs for the observation of very bright and faint targets. Table 1 summarizes operation and performance parameters for these modes.

Table 1. Parameters of the implemented polarization detector modes.

	Fast polarimetry	Fast window polarimetry	Slow polarimetry
science application	high precision polarimetry of targets with intermediate brightness (R ~ 3-7 mag) in broad band filters	highest precision polarimetry of the central PSF of the brightest targets (R < 3 mag) in broad band filters	photon noise limited polarimetry of faint targets, or bright star observations of the outer PSF or in narrow band filters
modulation: frequency, time	967 Hz, 1.03 ms		27 Hz, 37ms
row shift time (binned row)	54.7 µs		72.3 µs
Detector field of view*	3.5"×3.5", 1024 × 512 pix	1"× 1", 300 × 150 pix	3.5"× 3.5", 1024 × 512 pix
integration times: min-max	1.1 – 100 s	0.16 – 10 s	10 – 1000 s
frame transfer time	56 ms	20 ms	74 ms
max. frame rate	0.86 Hz	5.3 Hz	0.1 Hz
Shutter use	yes or no		No
read-out: noise, frequency	20e$^-$, 625 kHz		3e$^-$, 100 kHz
gain, well depth	10.5 e$^-$/ADU, 670 ke$^-$		1.5 e$^-$/ADU, 100 ke$^-$
dark current	0.2 e$^-$/(s pix)		0.015 e$^-$/(s pix)

* effective field of view for one polarization mode I_0 or I_{90}.

Bright targets need a fast modulation (~1 kHz) to freeze the speckle noise, a high frame rate (~1 s^{-1}) and a high full well capacity (> 10^5) per pixel to collect a lot of photons for high precision polarimetry. With a pixel read frequency of 625 kHz about half a line plus some pre- or overscan can be read-out during half a modulation cycle. A line read-out includes the registration of a first section of a line, then the read-out is stopped to allow for the row shift in the image area, before

the line read-out is completed. In this way, it is possible to read one line per full modulation cycle or 1 frame in a bit more than 1s. A higher frame rate is achieved by restricting the read-out to a window of 446 × 300 pixels and partial frame-transfers for smaller overheads. One row of this window can be read during half a modulation cycle (~0.5 ms) and the whole window is registered in about 0.16 s. The window mode requires special focal plane masks with an aperture of 1" × 1" to avoid unwanted illumination (e.g. frame n+1 in Figure 3 should not be illuminated).

The polarimetry of fainter targets is limited by photon noise. Therefore faint targets require long integration times, low read-out noise and dark current, while the polarimetric modulation can be slow. A half cycle in slow modulation lasts about 18ms, during which 2 detector lines can be read with low read-out noise. Thus, one frame can be registered in a bit less than 10s.

4.   POLARIZATION EFFICIENCY – DETECTOR EFFECTS

A perfect polarimetric system measures the polarization signal with an efficiency $\varepsilon_{pol} = 1$. In the ZIMPOL / SPHERE fast modulation - demodulation polarimetric system, this efficiency is limited by the following effects:

- The switch of the photo-electric polarimetric modulation and the charge-shifting demodulation require both a finite time of about 50 to 80 µs. In addition, small synchronization errors may cause an additional efficiency loss. This reduces the temporal efficiency to about $\varepsilon_{time} \approx 0.90$ for fast modulation, while $\varepsilon_{tim} > 0.99$ for slow modulation.

- Static charge and light leakage on the masked CCDs from the illuminated pixel rows to the covered buffer rows during the integration phase. This introduces an efficiency factor of about $\varepsilon_{mask} \approx 0.95$.

- The polarimetric properties of the modulator and the polarization beam-splitter are not perfect introducing a static efficiency factor for the modulation of about $\varepsilon_{mod} \approx 0.95$[15].

- The optical components of the telescope and instrument introduce a small efficiency loss due to polarization cross talks e.g. from linear to circular polarization. The corresponding efficiency factor is roughly $\varepsilon_{opt} \approx 0.98$.

All these effects must be considered as multiplicative factors $\varepsilon_{pol} = \varepsilon_{time}\ \varepsilon_{mask}\ \varepsilon_{mod}\ \varepsilon_{opt}$. The resulting polarization efficiency is at the level $\varepsilon_{pol} \approx 0.80$ for fast polarimetry and $\varepsilon_{pol} \approx 0.90$ for slow polarimetry. In this paper we discuss in more detail the polarization efficiency factors related to the detector effects mentioned in the first two points above.

4.1 Efficiency loss due to charge shifting and synchronization errors

We can estimate the efficiency loss introduced by the finite time required for the polarimetric modulation and demodulation with a simple model (Figure 4). The modulator switch can be described by a linear transition with a switch time Δt_{switch} between full and zero transmission of a fully polarized signal $f_{mod}(t)$. Similarly the charge shifting and the exposure of the two image planes $e_0(t)$ and $e_{90}(t) = 1 - e_0(t)$ can be treated as a linear transition with a time scale Δt_{shift} between zero and full illumination. In addition, we can also consider a time delay Δt_{delay} between modulation and demodulating. The created photo-charges are then given by $i_0(t) = f_{mod}(t)\ e_0(t)$ and $i_{90}(t) = f_{mod}(t)\ e_{90}(t)$ for the two image planes and the integration over one (or many) full modulation cycle yields then the registered signal I_0 and I_{90}. The resulting temporal efficiency is then

$$\varepsilon_{time} = |I_0 - I_{90}| / (I_0 + I_{90}) \ .$$

In the ZIMPOL / SPHERE case, the measured modulator switch time is about $\Delta t_{switch} = 75$ µs and the charge shift time $\Delta t_{shift} = 55$ µs. Adopting the simple model above gives for the zero time delay case $\Delta t_{delay} = 0$ an efficiency $\varepsilon_{time} = 0.915$.

The temporal efficiency ε_{time} for fast polarimetry can be derived with a comparison of the measured total efficiency ε_{pol} for fast and slow modulation mode. The polarization efficiency can be split into temporal and static contributions $\varepsilon_{pol} = \varepsilon_{time}\ \varepsilon_{static}$, where $\varepsilon_{static} = \varepsilon_{mask}\ \varepsilon_{mod}\ \varepsilon_{opt}$ are equal in both modes. ε_{time} for slow polarimetry is essentially equal to 1 because the efficiency losses are of the order $\approx \Delta t/t_{cycle}$. Since the cycle time t_{cycle} is 36 times longer for slow polarimetry the impact of the timing effects on the polarimetric efficiency are much reduced and can be neglected for slow polarimetry.

In our November 2011 test run we obtained for R and I band filters and CCD1 a total modulation – demodulation of about 91.5% ($\approx \varepsilon_{static}$) in slow polarimetry and 84.4% ($= \varepsilon_{pol}$) in fast polarimetry. This indicates that the timing efficiency in fast polarimetry is $\varepsilon_{time} = 0.927$ slightly higher than derived with our simple modeling. It is likely that the adopted shift time $\Delta t_{shift} = 55$ µs and the linear transition does not account for the stripe mask overlap of 1/3 of a row. If we shorten $\Delta t_{shift} = 36$ µs in the model then we obtain $\varepsilon_{time} = 0.922$ in good agreement with our simple modeling. In any case, our tests show that the results are near expectations.

With the simple model, we can also investigate the impact of a possible synchronization error between modulation and charge-shifting. Again using the parameters from the fast modulation model one gets a timing efficiency of $\varepsilon_{time} = 0.915$ for zero time delay, $\varepsilon_{time} = 0.909$ for $\Delta t_{delay} = 10$ µs, $\varepsilon_{time} = 0.893$ for $\Delta t_{delay} = 20$ µs, and $\varepsilon_{time} = 0.868$ for $\Delta t_{delay} = 30$ µs.
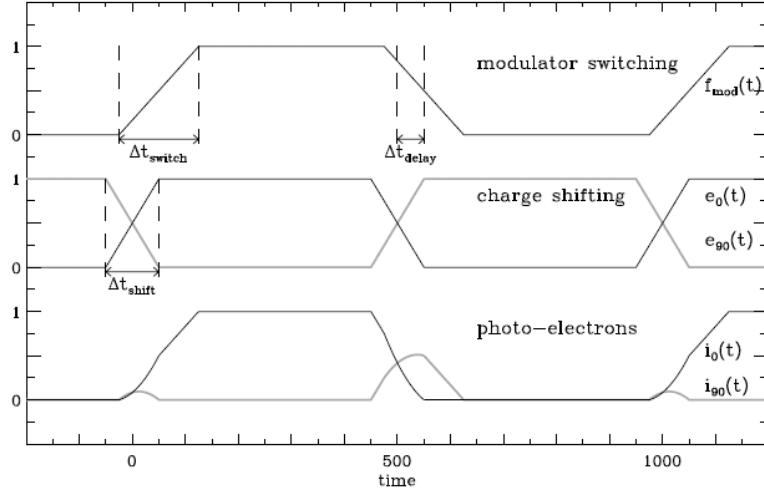
Figure 4. Schematic illustration of the timing parameters involved in the modulation – demodulation effects. The cycle time is 1000 units. In this figure the modulator switch time Δt_{switch}, the charge shift time Δt_{shift} and the synchronization delay time Δt_{delay} are exaggerated with respect to the ZIMPOL fast polarimetry timing.

4.2 Static charge and light leakage

The mask efficiency ε_{mask} accounts for the static charge and light leakage from the open, illuminated rows to the covered rows during the integration phase. These effects depend on the mask geometry and the detector pixel-to-pixel cross talk. One can distinguish between:

- Light pollution describes the light which produces photo-electrons in the covered rows instead of the illuminated open rows because of light scattering or diffraction on the stripe mask. Another possibility is, particularly for longer wavelengths, that the photons penetrate through the Si detector layer down to the electrodes of the back-illuminated CCD and are reflected or scattered to the neighboring covered pixel row.

- Charge diffusion are photo-charges created in the detector surface layer quite far above the pixel electrodes (especially for short wavelength photons) of the back-illuminated CCD or near a pixel boundary which may diffuse to the "wrong" pixel because the electric potential is not strongly dominated by one pixel.

Both effects are reduced with a large overlap of the occulting mask over the boundaries of the pixel rows that have to be hidden from light. Our study of candidate CCDs showed that a high mask efficiency ε_{mask} can be achieved with the chosen 2k × 2k pixel CCD which is used as a 1k × 1k pixel CCD with 2 × 2 binned pixels with an effective pixel size of 30 µm × 30 µm and a stripe mask with an overlap of 5 µm on each side.

The charge and light leakage effects can be accurately measured with flat field observation in standard imaging mode thus using a detector mode without charge-shifting. This imaging mode provides besides the (strong) illumination in the

open rows also a weak signal in the covered rows which is due to the charge and light leakage effect. We have measured this leakage as ratio $R=I_{cov}/I_{open}$ for different filters with the following detector averaged results:

- for CCD1, the ratios are R = 4.4%, 3.3% and 2.6% for the V, R and I pass-bands,

- for CCD2, R = 5.1%, 3.7% and 3.0% for the V, R and I pass-bands.

These values indicate that the charge and light leakage is stronger for short wavelength mainly due to the larger pixel to pixel crosstalk of the CCDs. We also observe a slightly lower performance for CCD2 which can be explained by less accurate alignment of the stripe mask / micro-lens array. Further we observe slight differences of the leakage for different detector regions because the CCDs have a surface height variation of a few μm with corresponding variations in the gap between mask and detector and variations of the stray light pollution. Gluing the micro-lens mask directly onto the CCD would improve the situation but introduces a significant risk of damaging the CCD in the alignment process.

The impact of the leakage on the mask efficiency can be deduced according to:

$$\varepsilon_{mask} = (I_{open} - I_{cov}) / (I_{open} + I_{cov}) \ ,$$

giving roughly $\varepsilon_{mask} \approx 0.95$ for a leakage of R = 2.5%.

5. CHARGE TRAPS AND TWO-PHASE DEMODULATION MODE

Charge traps are a critical detector effect for the demodulation because the up and down shifting of charges can cause strong pocket pumping. For example a charge trap can hold one electron during a down shift and then releases it in the following up-shift. In this way, a trap will dig after 1000 shifts a hole of 1000 e$^-$ in the image of one modulation phase, say I_0, and produce a spike of 1000 e$^-$ in the other modulation phase I_{90}. It was demonstrated by D. Gisler and collaborators[9] that this problem can be solved with a phase switching. For every second frame, the charge shifting is reversed with respect to the polarization modulation so that the charge trap pattern is cancelled in a double difference:

$$2Q = 2 (I_0 - I_{90}) = (I_{odd}(0) - I_{even}(0)) - (I_{odd}(\pi) - I_{even}(\pi)) \ ,$$

where I_{odd} and I_{even} are the counts registered in the odd and even detector rows for either 0- or π-phase shift between modulation and demodulation.

Figure 5 shows a test of the charge trap correction procedure for data taken with ZIMPOL in Nov. 2011 in fast polarimetry mode for a 5% polarized flat-field illuminations of about $2 \ 10^5$ e$^-$/pixel. Only the normalized counts of one line of CCD1 are shown. Because of the polarized illumination every second (even) pixel in the selected 0-phase frame has a 10% higher count rate than the odd pixels. Three frames with increasing integration times equivalent to more charge transfer shifts are shown, a 1.2s integration with about 10^3 modulation cycles, a 10s integration with about 10^4 cycles taken with a ND1 filter, and a 100s integration with about 10^5 modulation cycles taken with a ND2 filter. It is clearly visible that the charge traps grow together with the number of charge shifting cycles. For the 100s integration also the π-phase counts are shown with the same spurious charge traps but with the polarization signal reversed. A simple difference of the 0-phase and π-phase pixel counts removes the charge trap features in the differential polarization signal but not in the summed intensity signal.

From our tests, we can highlight a few results about the charge trap frequency and strengths. For both CCDs similar statistical results are obtained. About 2% of all pixels show a charge trap deviation of 2% from the mean value after 10^4 modulation cycles. The column displayed in Figure 5 shows three pixels which do not obey the periodic pattern. After 10^5 modulation cycles these charge traps have grown to strong deviations from the periodic pattern and the number of all traps which generate at least a 2% deviations from the median is about 5 – 10%. This is a substantial fraction of all pixels but their effect can be well corrected with the double difference method. Although of interest for an optimal selection of the detector mode parameters, it is beyond the scope of this paper to discuss the charge trap properties in more detail.

The charge traps have an important impact on the polarimetric detector operation modes of ZIMPOL: because of the charge traps the phase shift is implemented in all polarimetric detector modes. For the user it is only possible to take an even number (at least two) of identical exposures, so that the "0-phase minus π-phase" double difference charge trap correction can be applied to the evaluation of the differential signal of consecutive frames in the data reduction.
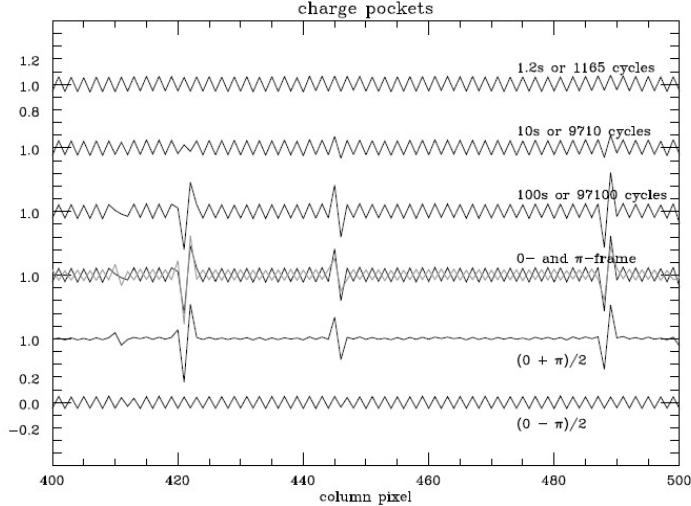
Figure 5. Normalized count rates for pixels in column 90 of a raw flat-field frame from CCD2 taken in fast polarimetry mode with 1.2s, 10 s, and 100s integrations. The forth line from the top shows the signal in the 0-phase and π-phase for the 100s integration and the next lines the summed up intensity $(0 + \pi)$ and the differential polarization signal $(0 - \pi)$. The two-phase demodulation removes essentially all charge pocket effects.

6.   BIAS LEVEL, DARK CURRENT AND READ OUT PATTERNS

6.1 Bias frames and pre- and overscan bias level

All science exposures and calibration frames for ZIMPOL polarimetry are taken as one or many pairs of consecutive frames. Therefore even a bias frame includes an integration phase, when the previous frame is read out (or a dummy frame for the first frame of a data series). This implies that there are no real bias frame pairs or ``zero second'' integration frame pairs can be taken with the ZIMPOL CCDs. What we call a bias frame is in principle a short dark frame of 1.1s in fast polarimetry and 10s in slow polarimetry. For fast window polarimetry, the situation is even more complicated because one frame is "on the CCD" during the read-out of the previous three frames lasting each 0.16s or a minimum integration of 0.48ms (Figure 3**).** Besides the read-out, there is also one frame transfer involved in full frame fast and slow polarimetry mode and three partial frame transfers in fast window polarimetry mode.

We measured for the ZIMPOL detector modes bias level variations of a few ADUs. Such variations seem to be unavoidable considering the "heavy duty" character of the simultaneous demodulation and read-out implemented for the ZIMPOL CCD operation modes. Because of the high gain of 10.5 e⁻/ADU for the fast modulation modes, a bias drift of 3 ADUs corresponds to roughly 30 e⁻. Since adjacent odd and even detector rows have the same bias level, any bias level variation is automatically corrected in the $Q = I_{odd} - I_{even}$ subtraction for the evaluation of the differential polarization. However for the intensity signal, an unaccounted bias level drift may affect significantly the background correction in the science frame and the evaluation of the dark current measurements.

For the ZIMPOL CCD detector modes, the bias drift problem is mitigated by including always pre- and overscan pixels in the read-out process. The registered raw data have therefore a format with two image areas from the two read-out registers separated by 2×41 overscan-pixels in the middle and 25 pre-scan pixels at the beginning and end of each line. Figure 6 shows a 100s dark exposure of full frame fast polarimetry of CCD1 which illustrates well the raw data format.

6.2 Read-out stop column in full frame fast polarimetry

In fast polarimetry full frame mode there are two columns per CCD with strongly different bias level. They originate from the interruption of the line read-out process after 266 pixels in order to allow for a line shift in the image area

without introducing electronic pick up noise in the data. The bias level in these two columns is strongly enhanced for the 0-phase frame with about 500 and 300 ADU counts above the mean bias level in CCD1 and CCD2 respectively (see Figure 6) and slightly reduced in the π-phase frame with about 20 ADU and 75 ADU below the mean bias level. The differences in the 0- and π-phase frames have most likely its origin in the opposite charge shift direction during the read-out stop and therefore a reversed voltage pattern applied to the 3 phases of the image area affecting the read-out bias level of the ``stop pixels'' in a different way.

For the differential polarimetry Q the enhanced ADU level for the read-out column is just canceled with the double difference. For the intensity image I the stop columns are corrected in the bias subtraction procedure.
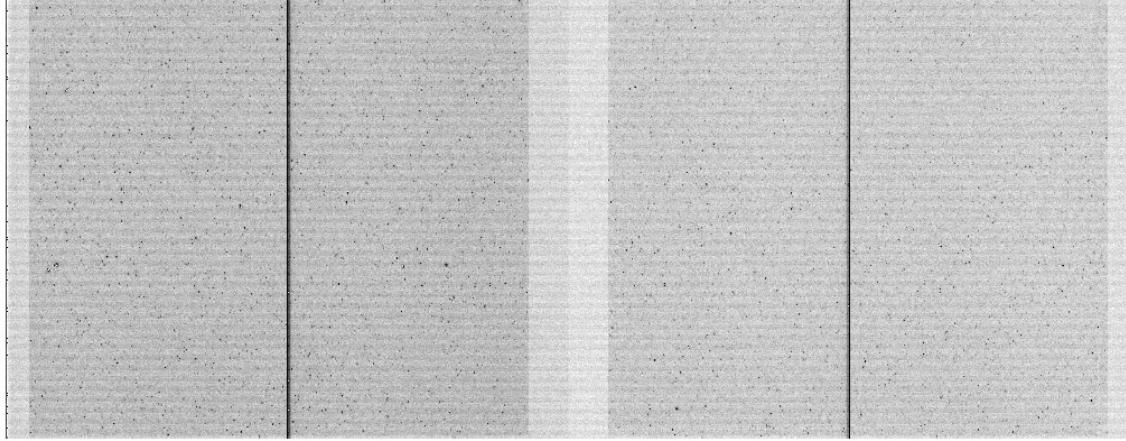

Figure 6. A 1156 × 400 section of a 100s 0-phase dark frame taken in full frame fast polarimetry mode. The right and left side are read out by different read-out registers. The left side is slightly darker because the bias level is on average 2 ADU counts higher. From the outside border there are first two 25 pre-scan pixel columns, then the two slightly darker image areas with 512 columns with a dark current signal of about 5 ADU counts with the very bright (black) read out stop columns, and in the middle two regions with 42 over-scan columns each.

6.3 Read-out noise

Image areas with no or only a low illumination level show a stripe pattern in row direction with a periodicity of about 9 pixel which is probably due to electronic pick-up noise. In Figure 6, this effect is visible as straight horizontal lines running over the entire image. However, the amplitude of this periodic pattern is only about 1 ADU and therefore it disappears as soon as some illumination with photon noise is present. The pattern shifts up or down from exposure to exposure and therefore the averaging of many frames reduces the effect on a relative scale. The measured standard deviation for the pixel to pixel read-out noise is about 2 – 3 ADUs including the horizontal line pattern described above but not the pixels of the read-out stop column. If only the pixels of a read-out stop column are considered, then the pixel to pixel read-out noise is the same, only the mean value is (strongly) different.

For the high flux applications foreseen for ZIMPOL / SPHERE the read-out, bias and dark current characteristics measured during the instrument testing phase are all very good and we expect no impact on the science data quality from the effects described in this section.

7. FRAME TRANSFER SMEARING

Before and after each detector illumination a fast frame transfer takes place which moves an illuminated frame from the image area down into the read-out area and a new image ``from above'' into the image area. During this phase, light falls onto the CCDs if no shutter is used. This illumination introduces a smearing of the image in column direction. All pixels P_{ij} in a given column i (read-out direction) receive the same amount of light from the frame transfer process, which is

proportional to the summed light of all pixels in the column $f_{i,smear} = c_{smear} \Sigma_j P_{ij}$. The parameter c_{smear} describes the dependence of this effect on frame transfer time t_{ft} and integration time t_{exp} according to

$$c_{smear} = t_{ft} / t_{exp}.$$

This indicates that the frame transfer smearing is important for short integrations. Maximum values are $c_{smear} = 0.125$ for a 160 ms integration for fast modulation window mode, 0.051 for a 1.1s fast modulation full frame integration, and 0.0074 for a 10s slow modulation frame.

The frame transfer smearing adds a level of background, similar to scattered light to the image. The effect is most obvious for short integration of bright sources which produce a trail in column direction. The differential polarization signal Q is not affected by this smearing but it adds of course additional photon noise, which can be substantial if an interesting source is located on the frame transfer trail of a bright star. For the intensity signal, an additional reduction step is required to subtract the frame transfer smearing signal.

To avoid the smearing effect and to enhance the performance of ZIMPOL, a shutter is available for fast polarimetry modes which stops the light during the frame transfer phase. The shutter requires about 5-10 ms to close or open reducing the effective exposure time by only a small amount. Thus the shutter can be quite useful for reducing the additional background due to frame transfer smearing. However, the shutter introduces also some risks. It may produce mechanical vibrations in the system and cause disturbing air turbulence in the optical path. Both effects are hard to estimate and we need further testing to investigate this. Further one should also consider, that the expected lifetime of the shutter is limited if millions of short integrations (e.g. at a cadence of 10'000 cycle per hour) are taken. For these reasons it is always possible to operate the polarimetric detector modes also without shutter, accepting some enhanced background due to frame transfer smearing.

8. CONCLUSIONS

This paper describes the basic concept of the demodulating CCDs used in the ZIMPOL imaging polarimeter for the high contrast search of reflected light from planetary systems with SPHERE at the VLT. The ZIMPOL concept is an innovative and quite complex technique for polarimetric measurements. The ZIMPOL fast modulation technique is implemented in SPHERE because it provides a differential technique which freezes the speckle noise and any other temporal changes in the measuring process. This provides a key advantage for the detection of polarized (= reflected) light from circumstellar targets.

The tests presented in this work for the ZIMPOL demodulating CCD detector system demonstrate that the system works well. The achievable polarimetric efficiency is within the specifications and potentially harmful detector effects are under control. In particular the charge trap effects can be corrected well with the two-phase demodulation mode. Bias level variations can be taken into account using pre- and overscan pixel read-outs. Read-out patterns are either stable and can be corrected in the data reduction or they are at a level which can be neglected.

The ZIMPOL CCDs performed also very well in the high performance tests of the ZIMPOL subsystem[12]. These tests showed that a polarimetric sensitivity of 10^{-5} can be achieved with these detectors for ``flat field'' illuminations and that a very weak polarimetric signal can be detected near a very bright point source. The most important next step is now the evaluation and definition of the best detector operation strategies for the different science applications with further testing in the laboratory using the SPHERE AO system and with on-sky tests.

REFERENCES

[1] Beuzit, J.L., Feldt, M., Dohlen, K., Mouillet, D., Puget, P. and SPHERE Consortium, "SPHERE: a Planet Finder instrument for the VLT." ESO Messenger 125, 92

[2] Beuzit, J.L., Feldt, M., Dohlen, K., Mouillet, D., Puget, P., Wildi, F.P., and SPHERE Consortium, "SPHERE: a Planet Finder instrument for the VLT," Proc. of SPIE Vol. 7014, Paper 701418 (2008)

[3] Schmid, H.M., Beuzit, J.L., Feldt, M., Gisler, D., Gratton, R., Henning et al., "Search and investigation of extra-solar planets with polarimetry," IAU Coll. 200, 165–170 (2006)

[4] Kemp, J.C., "Piezo-Optical Birefringence Modulators: New Uses for a Long-Known Effect," Jour. Opt. Soc. America 59, 950 (1969)

[5] Kemp, J.C., Barbour M.S., "A photoelastic-modulator polarimeter at Pine Mountain observatory," PASP 93, 521 (1981)

[6] Povel, H.P., Aebersold, F., and Stenflo, J., "Charge-coupled device image sensor as a demodulator in a 2-D polarimeter with a piezoelastic modulator," Appl. Opt. 29, 1186 (1990)

[7] Povel, H.P., "Imaging Stokes polarimetry with piezoelastic modulators and charge-coupled-device image sensors," Optical Engineering 34, 1870 (1995)

[8] Stenflo, J.O., Keller, C.U., "New Window for Spectroscopy," Nature 382, 558 (1996)

[9] Gisler, D., Schmid, H.M., Thalmann, C., Povel, H.P., Stenflo, J.O., Joos, F., et al., "CHEOPS/ZIMPOL: a VLT instrument study for the polarimetric search of scattered light from extrasolar planets," Proc. of SPIE Vol. 5492, 463-474 (2004)

[10] Thalmann, C., Schmid, H.M., Boccaletti, A., Mouillet, D., Dohlen, K., Roelfsema, R., Carbillet, M., et al., "SPHERE ZIMPOL: overview and performance simulation," Proc. of SPIE Vol. 7014, 70143F (2008)

[11] Roelfsema, R., Schmid, H.M., Pragt, J., Gisler, D., Waters, R., Bazzon, A., et al., ``The ZIMPOL high-contrast imaging polarimeter for SPHERE: design, manufacturing, and testing", Proc. of SPIE Vol., 7735, 77354B (2010)

[12] Roelfsema, R., Gisler, D., Pragt, J., Schmid, H.M., Bazzon A., Dominik C., et al., "The ZIMPOL high contrast imaging polarimeter for SPHERE: sub-system test results," Proc. of SPIE Vol. 8151, 81510N (2011)

[13] Pragt, J., Roelfsema, R., Gisler, D., Wildi, F., Schmid, H.M., Rigal, F. et al., "Alignement of the SPHERE-ZIMPOL polarimeter," Proc. of SPIE Vol. 8446, submitted (2012)

[14] Wildi, F., Beuzit J.L., Feldt, M., Mouillet, D., Dohlen, K., Puget, P., et al., ``The performance of the SPHERE sub-systems in the integration lab'', Proc. of SPIE Vol. 8151, 81510M (2011)

[15] Bazzon, A., Gisler, D., Roelfsema, R., Schmid, H.M., Pragt, J. Elswijk, E., et al., "SPHERE/ZIMPOL: Laboratory tests oft he optical polarization components," Proc. of SPIE Vol. 8446, submitted (2012)